the target every four reaches, effectively switching the direction of the prismatic displacement and preventing complete adaptation to either orientation.

Error-correction task. Goggles contained clear lenses rather than prisms and subjects alternated the viewing eye as they had in the adaptation condition. As a subject began his reach, however, the target location suddenly shifted by 7 cm either to the right or to the left of the initial position, thereby requiring the subject to make a trajectory correction during the reach. The magnitude of the target shift was roughly the same as the visual displacement produced by the prisms, and resulted in reaching movements with the same curved hand paths that were observed in the adaptation task. Using an analysis of variance, which effectively subtracted the error-correction from the prism-adaptation images, activations relating to limb movements, to visual and sensory conditions, and to error-correction processes were effectively removed, leaving only those activations that were related to the adaptive process itself.

Positron-emission tomography. Scans were done with a Siemens ECAT EXACT scanner with septa retracted to allow three-dimensional imaging. A series of 90-s scans were made from each subject, using bolus intravenous injections of $H_2{}^{15}O$ (25 mCi) that were delivered before the start of each scan. Performance of the designated task began at the same time as the tracer injection, and the scanning period began 10 s after injection. The subject completed 21 or 22 reaches during each 90-s scanning period. High-resolution magnetic resonance images of each subject's brain were obtained in separate sessions (2.5 mm contiguous T1-weighted transaxial spin-echo images (256×256 matrix size, time of repetition (TR) = 650 ms, time of echo (TE) = 20 ms) performed on a Philips NT scanner) for individual coregistration with the PET images[26,27]. PET images were reconstructed with a ramp filter and then smoothed in three dimensions using a Hanning filter with a cut-off frequency of 1 cycle per cm. The final isotropic resolution of the filtered images was 11.2 mm full width at half maximum height. To permit intersubject comparisons, each subject's coregistered PET images were then mapped into the standard Talairach coordinate space. Separate three-way ANOVAs were done (with factors being task, subject and replication), and then contrast analyses were used to produce *t*-statistic images based on comparisons across pairs of conditions (for example, prism adaptation minus error correction)[28,29]. To minimize type I errors, the search region was restricted to functionally plausible structures, including contralateral sensorimotor, premotor and posterior parietal cortex, and ipsilateral cerebellum. Areas of focal activation that were detected on the *t*-thresholded images were subjected to an analysis of cluster-based significance to calculate corrected *P* values for each activation site[30]. This analysis was sensitive to the extent as well as the intensity of activation, and corrected for the fact that multiple *t* statistics were generated within the area of search.

Received 7 June; accepted 22 August 1996.

1. Kalaska, J. F. & Crammond, D. J. *Science* **255,** 1517–1523 (1992).
2. Georgopoulos, A. P. *Annu. Rev. Neurosci.* **14,** 361–377 (1991).
3. Redding, G. M. & Wallace, B. *Percept. Psychophys.* **44,** 59–68 (1988).
4. Welch, R. B., Choe, C. S. & Heinrich, D. R. *J. Exp. Psychol.* **103,** 700–705 (1974).
5. Redding, G. M., Clark, S. E. & Wallace, B. *Cogn. Psychol.* **17,** 1–25 (1985).
6. Wilkinson, D. A. *J. Exp. Psychol.* **89,** 250–257 (1971).
7. Baily, J. S. Q. *J. Exp. Psychol.* **24,** 8–20 (1972).
8. Choe, C. S. & Welch, R. B. *J. Exp. Psychol.* **102,** 1076–1084 (1974).
9. Beckett, P. A. *J. Exp. Psychol.* **6,** 433–444 (1980).
10. Eidelberg, D. & Galaburda, A. M. *Arch. Neurol.* **41,** 843–852 (1984).
11. Seltzer, B. & Pandya, D. N. *Brain Res.* **192,** 339–351 (1980).
12. Colby, C. L., Duhamel, J. R. & Goldberg, M. E. *J. Neurophysiol.* **69,** 902–914 (1993).
13. Thach, W. T., Goodkin, H. P. & Keating, J. G. *Annu. Rev. Neurosci.* **15,** 403–442 (1992).
14. Zeffiro, T. *Hum. Brain Mapp.* suppl 1, 333 (1995).
15. Grafton, S. T., Mazziotta, J. C., Woods, R. P. & Phelps, M. E. *Brain* **115,** 565–587 (1992).
16. Kawashima, R., Roland, P. E. & O'Sullivan, B. T. *J. Neurosci.* **14,** 3462–3474 (1994).
17. Deiber, M. P. *et al. Exp. Brain Res.* **84,** 393–402 (1991).
18. Stephan, K. M. *et al. J. Neurophysiol.* **73,** 373–386 (1995).
19. Bonda, E., Petrides, M., Frey, S. & Evans, A. *Proc. Natl Acad. Sci. USA* **92,** 11180–11184 (1995).
20. Parsons, L. M. *et al. Nature* **375,** 54–58 (1995).
21. Corbetta, M., Miezin, F. M., Shulman, G. L. & Petersen, S. E. *J. Neurosci.* **13,** 1202–1226 (1993).
22. Corbetta, M., Shulman, G. L., Miezin, F. M. & Petersen, S. E. *Science* **270,** 802–805 (1995).
23. Pardo, J. V., Fox, P. T. & Raichle, M. E. *Nature* **349,** 61–64 (1991).
24. Talairach, J. & Tournoux, P. *Co-Planar Stereotaxic Atlas of the Human Brain* (Thieme, New York, 1988).
25. Perenin, M. & Vighetto, A. *Brain* **111,** 643–674 (1988).
26. Woods, R. P., Cherry, S. R. & Mazziotta, J. C. *J. Comput. Assist. Tomogr.* **16,** 620–633 (1992).
27. Woods, R. P., Mazziotta, J. C. & Cherry, S. R. *J. Comput. Assist. Tomogr.* **17,** 536–546 (1993).
28. Neter, J., Wasserman, W. & Kutner, M. H. *Applied Linear Statistical Models* (Irwin, Burr Ridge, Illinois, 1990).
29. Woods, R. P., Iacoboni, M., Grafton, S. T. & Mazziotta, J. C. in *Quantification of Brain Function Using PET* (eds Meyers, R., Cunningham, V. & Bailey, D.) 353–358 (Academic, New York, 1996).
30. Friston, K. J., Worsley, K. J., Frackowiak, R. S. J., Mazziotta, J. C. & Evans, A. C. *Hum. Brain Mapp.* **1,** 210–220 (1994).

ACKNOWLEDGEMENTS. This work was supported in part by the PET Imaging Center, Emory University School of Medicine, Georgia and by grants from the National Institutes of Health. We thank S. T. Grafton for helpful discussions and for his critical reading of the manuscript.

CORRESPONDENCE and requests for materials should be addressed to G.E.A. (e-mail: gea@neuro.emory.edu).

A mechanism for generation of long-range synchronous fast oscillations in the cortex

Roger D. Traub*†, Miles A. Whittington‡, Ian M. Stanford§ & John G. R. Jefferys§

* IBM Research Division, T. J. Watson Research Center, Yorktown Heights, New York 10598, USA
† Department of Neurology, Columbia University, New York, New York 10032, USA
‡ Department of Physiology and Biophysics, Imperial College School of Medicine at St Mary's, London W2 1PG, UK
§ Department of Physiology, The Medical School, University of Birmingham, Birmingham B15 2TT, UK

SYNCHRONOUS neuronal oscillations in the 30–70 Hz range, known as gamma oscillations, occur in the cortex of many species[1–6]. This synchronization can occur over large distances, and in some cases over multiple cortical areas[7,8] and in both hemispheres[2]; it has been proposed to underlie the binding of several features into a single perceptual entity[4]. The mechanism by which coherent oscillations are generated remains unclear, because they often show zero or near-zero phase lags over long distances, whereas much greater phase lags would be expected from the slow speed of axonal conduction. We have previously shown that interneuron networks alone can generate gamma oscillations[9,10]; here we propose a simple model to explain how an interconnected chain of such networks can generate coherent oscillations. The model incorporates known properties of excitatory pyramidal cells and inhibitory interneurons; it predicts that when excitation of interneurons reaches a level sufficient to induce pairs of spikes in rapid succession (spike doublets), the network will generate gamma oscillations that are synchronized on a millisecond timescale from one end of the chain to the other. We show that in rat hippocampal slices interneurons do indeed fire spike doublets under conditions in which gamma oscillations are synchronized over several millimetres, whereas they fire single spikes under other conditions. Thus, known properties of neurons and local synaptic circuits can account for tightly synchronized oscillations in large neuronal ensembles.

In visual cortex, gamma oscillations can be evoked by visual stimulation. When the stimulus is topologically connected (a long bar, for example), the oscillations can be coherent over distances of up to 7 mm, with zero or near-zero (<3 ms) average phase lag[1]. Coherence of in-phase gamma oscillations has also been observed between primary and associational visual cortices[7,8], and across the corpus callosum[2], where antidromic axonal conduction delays are estimated to be 2.73 ± 2.38 ms (ref. 11). In humans, gamma oscillations are observed in magnetic signals emanating from large regions of cerebral cortex and subcortical structures[12]. The mechanism of coherence is not obvious, as axonal conduction in local circuit axonal processes is slow (~0.5 m s^{-1}, or 1 cm in 20 ms, for hippocampal Schaffer collaterals[13]; 0.15–0.55 m s^{-1} for neocortical pyramidal cell collaterals[14]; and 0.06–0.2 m s^{-1} for neocortical inhibitory collaterals[15]).

The coherent oscillation problem can be broken down into two questions: how do local circuits, or even individual cells[16], generate gamma-frequency oscillations, and what happens when oscillating local circuits are synaptically interconnected? We begin with a known local-circuit interneuron network gamma oscillator[9,10]. We then use simulations to review how this local circuit behaves when both pyramidal cells and interneurons are present, and go on to demonstrate how synaptically interconnected local circuits can produce in-phase oscillations over significant distances. In our model, synchronized oscillations are apparent in single trials (unlike the model of ref. 17), even when conduction delays total 20 ms from one end of a chain of oscilla-

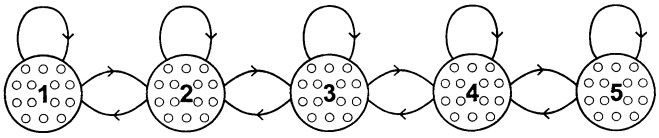

FIG. 1 Structure of the model. There are 5 cell groups, each with 8 pyramidal cells (e-cells, simulated as in ref. 26) and 8 basket cells (i-cells, simulated as in ref. 18). There are 4 types of synaptic connections: e → e (in some simulations), e → i, i → e, i → i. Connections occur between cells in each given group and between neighbouring groups, so that each cell has 16 excitatory and 16 inhibitory inputs. Inhibitory connections were $GABA_A$, with IPSCs of abrupt onset and exponential decay (τ = 10 ms). Excitatory connections were AMPA-receptor-mediated (conductance proportional to a 2-ms α-function between pyramidal cells, a 1-ms α function on i-cells) and NMDA-receptor-mediated (τ = 150 ms between pyramidal cells, 60 ms on i-cells). Peak unitary inhibitory conductances were 4 nS on e-cells, 1.5 nS on i-cells. Axon conduction delays within a group are considered negligible, whereas between groups they could range from 0 to 10 ms; in most simulations, intergroup conduction delays were 4 or 5 ms. Interneurons were biased with a small hyperpolarizing current to suppress spontaneous firing. Pyramidal cells received a somatic driving current of $1.6 + x$ nA, where x was varied over a 0.2 nA range across each group; there was an additional 0.01 nA spread across the cells, so that no 2 cells received identical currents. With such a current, isolated pyramidal cells would fire a single burst and then settle into a repetitive firing mode[26,27]. Data were collected for the last 750 ms of 1,500-ms runs. Noise was included in the form of ectopic action potentials in e-cell and i-cell axons. Simulations were run on IBM SP1 and SP2 parallel computers; a 1,500-ms simulation took 1.8 h on the SP2.

tors to the other. Finally, we provide experimental evidence for two central predictions of our model.

Local circuits of inhibitory interneurons—in hippocampus and neocortical layers 2/3 of the rat—can generate gamma-frequency oscillations during pharmacological blockade of ionotropic glutamate receptors, when the cells are excited by metabotropic glutamate receptors and inhibit each other by $GABA_A$ receptors[9]. A circuit model, using a 51-compartment axon/soma/dendritic model for each inter neuron[18], accounts for the observed properties of the network oscillation, including the dependence of network frequency on unitary inhibitory postsynaptic conductance and time course. The model works when a sufficiently high synaptic connectivity exists.[10,19]. This model also correctly predicts a break-up of the network oscillation when a sufficiently low frequency is attained[10]. In simulations, eight interneurons are sufficient to generate synchronized gamma oscillations, when all–all connectivity exists. In such small local circuits, axon conduction delays are probably negligible.

The behaviour of a local circuit generator of gamma oscillations was examined when pyramidal cells were included, with interneurons, using the following synaptic interactions: in the excitatory connection from pyramidal cells to interneurons, both slow (for example, NMDA-receptor-mediated) and fast (for example, AMPA-receptor-mediated) synaptic actions; and in the inhibitory connection from interneurons to other interneurons and to pyramidal cells, $GABA_A$-receptor-mediated synaptic action. Axon conduction delays were <0.5 ms for i-cells (inhibitory cells) and e-cells (excitatory or pyramidal cells) (R.D.T., J.G.R.J. and M.A.W., unpublished results). In this model, pyramidal cells and interneurons fired with near-zero phase lag on average, and on occasion the fast excitatory postsynaptic potentials (EPSPs) to interneurons induced doublet firing, at about 5-ms intervals, with the second interneuron spike usually following the pyramidal cell spike (see also Fig. 2*b*). (In the model, doublet firing did not occur as an intrinsic property of the interneurons.) This property of doublet firing suggested a way that oscillators might be connected together with conduction delays and still oscillate coherently with near-zero phase lag.

Figure 1 illustrates the structure of the model: a chain of five cell groups, each group containing eight pyramidal cells and eight interneurons, with all–all intragroup connectivity, and negligible intragroup axon-conduction delays. Cells in each group also receive excitatory and inhibitory input from one-half or all of the excitatory and inhibitory neurons in each neighbouring group, so that all cells have the same number of inputs. Conduction times for the intergroup excitatory and inhibitory axons were treated as free parameters and were manipulated independently (from 0 to 10 ms).

Figure 2*a* illustrates the behaviour of the network model when intergroup synaptic connections are cut. Individual cell groups oscillate at about 40 Hz, as seen in the autocorrelation, performed on the average of four pyramidal cell voltages from group 1, over a period of 750 ms. The flat intergroup cross-correlation shows that oscillations in the different ends of the chain are, on average, independent and uncorrelated; thus, there is no artefactual synchrony, as might exist in a noiseless system with identical stimuli to each group. Interneurons usually fire single action potentials, but spike doublets, synaptically induced, occur on occasion. Note that axo–axonic interneurons readily fire spike doublets during intracellular current injection[20], and it is not unusual for other interneurons, when sufficiently excited, to fire action potentials at short intervals[19].

In contrast (Fig. 2*b*), when intergroup synaptic connections are present, with 4-ms axon conduction delays between neighbouring

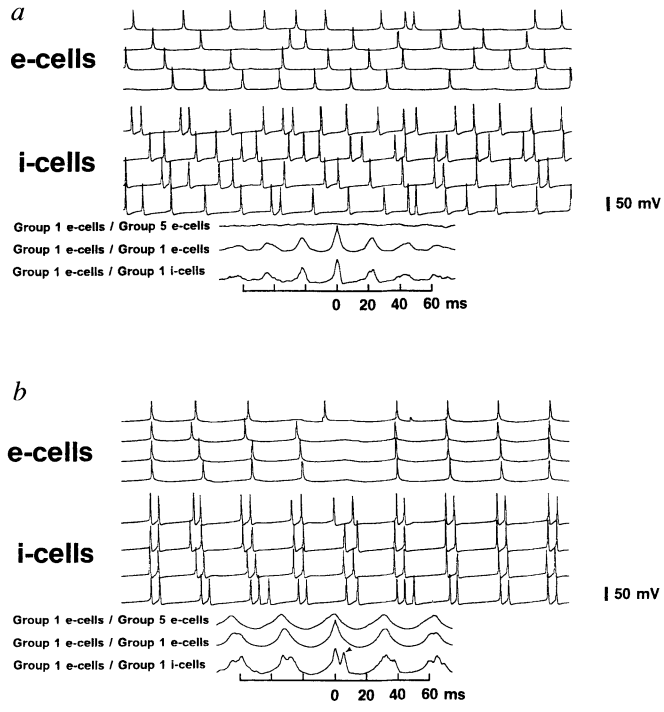

FIG. 2 Tight long-range synchronization exists in the model even with intergroup axon conduction delays. *a*, The 5-cell groups are uncoupled from each other. Potentials of 4 e-cells (top) and 4 i-cells (bottom) are shown; cells respectively from groups 1, 2, 4, 5. The autocorrelation and cross-correlation were obtained by averaging 4 e-cell potentials from groups 1 and 5. The group 1 autocorrelation reveals a peak at 25 ms (40 Hz), but the group 1/group 5 cross-correlation is flat. The group 1 e-cell/i-cell cross-correlation indicates that, on average, nearby e-cells and i-cells fire in phase. *b*, Same parameters as in *a*, but intergroup connections exist with axon conduction delays of 4 ms (e → i, i → e, i → i). The network frequency slows to 32 Hz, and tight correlations exist between groups 1 and 5 (the cross-correlation peak is at −0.9 ms). Note that now the interneurons fire mostly doublets at average 5.25-ms intervals. The group 1 e-cell/i-cell cross-correlation indicates that the first interneuron spike occurs with the same phase, on average, as the e-cell spike; doublet firing appears as the second peak, lagging the first peak by 5.25 ms; e → e connections were blocked in both simulations.

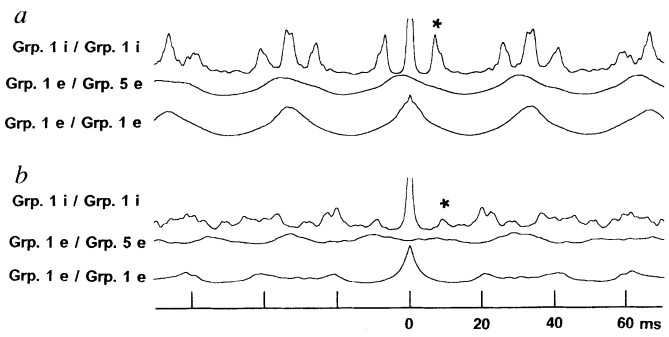

FIG. 3 Interneuron doublet firing is required for long-range synchronization in the model. *a*, When the e → i AMPA conductance is reduced to 50% of the value in Fig. 2, synchronized oscillations still occur (29 Hz), although now with a 2.5-ms lag in the e-cell cross-correlation (group 1/group 5). Interneuron doublet firing is indicated by the peaks (asterisk) around the (truncated) central peak in the interneuron autocorrelation (based on the average of 4 i-cell potentials from group 1). *b*, When the e → i AMPA conductance is further reduced to 24% of the value in Fig. 2, synchronized oscillations continue within individual cell groups (note the small but distinct 20 ms/50 Hz peak in the e-cell autocorrelation), but between-group correlations are lost. At the same time, doublet firing in interneurons is suppressed (asterisks in interneuron autocorrelation).

groups (hence 16 ms total delay between ends of the chain), coherent cellular oscillations occur throughout the system. The mean phase lag between opposite ends of the model chain is only 0.9 ms. The oscillation frequency also slows from 40 to 32 Hz. Note that in the simulation shown in Fig. 2*b*, the interneurons almost always fire in doublets or occasionally triplets.

To show that interneuron doublet firing provides the 'glue' that allows long-range synchronization to occur, we performed a manipulation to suppress doublet firing. In Fig. 3, the simulation of Fig. 2 was repeated twice, with progressively smaller values of the unitary e → i AMPA receptor conductance. When this conductance is still large enough for the second interneuron spike to be recruited, so for interneuron doublet firing to occur (Fig. 3*a*), strong correlations in cellular oscillations still occur from one end of the array to the other. As doublet firing is reduced sufficiently, long-range correlations in the oscillation are attenuated.

We next sought experimental evidence for interneuron doublets. Tetanic stimulation of the CA1 region of rat hippocampal slices is known to induce gamma-frequency synaptic potentials in pyramidal cells that are blocked by bicuculline and hence are probably generated by networks of inhibitory cells[9]. We found (Fig. 4) that simultaneous tetanic stimulation of two CA1 sites, at distances up to 4 mm apart, induces gamma-frequency field potential oscillations that are coherent (<1 ms phase lag in the cross-correlation). Physiologically identified stratum pyramidale interneurons fire rhythmic action potential singlets after local tetanic stimulation, whereas they usually fire doublets following double simultaneous tetanic stimulation (Fig. 4). Doublet firing was observed in 4 of 6 interneurons under such conditions. The oscillation frequency is reduced after the dual tetanic stimulation, as predicted by the model (Fig. 2). A similar reduction in gamma

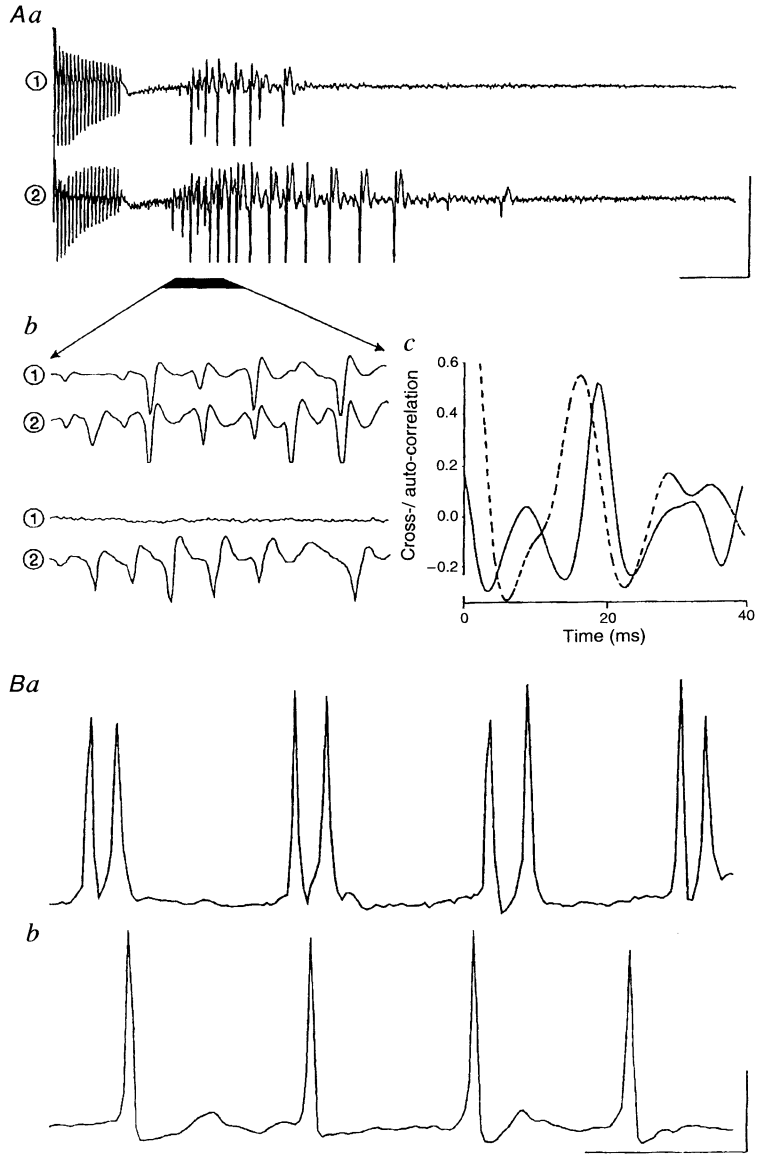

FIG. 4 Interneuron spike doublets occur under conditions ► associated with long-range synchrony in the hippocampal slice. *A*, Recordings of extracellular population potentials for two sites (1 and 2) in the hippocampal CA1 subfield separated by 4 mm. *a*, Trains of 20 stimuli sufficient to generate a half-maximal population spike were delivered at 100 Hz by bipolar electrodes placed at the border of stratum oriens/alveus at the CA2 (site 1) and subicular (site 2) ends of CA1. 50 to 150 ms following tetanus, rhythmic oscillating field potentials were seen in stratum pyramidale at both sites. Scale bar: 200 ms, 10 mV. *b*, Analysis of trains of oscillations at 2 sites revealed a highly synchronous organization of population spikes, with cross-correlation analysis showing a frequency of 52 Hz (cross-correlation, solid line). *c*, Single tetanic stimulation at site 2 also generated an oscillatory field potential locally, with a faster frequency of population spikes, 62 Hz (autocorrelation, broken line). Timescale was expended 7-fold for example traces. *B*, *a*, Recordings from electrophysiologically identified stratum pyramidale interneurons after paired tetanic stimulation revealed rhythmic doublet firing. *b*, Single-site tetanus generated interneuron oscillations locally with no doublet firing. Scale bar: 20 ms, 40 mV.

frequency oscillation with increasing size of the participating neuronal ensemble has been observed *in vivo*[21].

How might interneuron doublets permit long-range synchrony? König and Schillen[22] showed that global coherent oscillations can occur when a local circuit time constant matches the delay time between neighbouring local circuits. They unrealistically assumed, however, that the delay between pyramidal cell firing and excitation of nearby interneurons should match the conduction delay between separated cell groups. Doublet firing of the interneurons circumvents this need for slow conduction in the local circuit. Instead, the doublet interval of 4–5 ms acts as the local circuit time constant, which can then match approximately the conduction delay between spatially separated circuits. The second interneuron spike in each doublet is stimulated in part by nearby pyramidal cells and in part by the delayed excitation from spatially separated pyramidal cells. Synchronization between two model columns with conduction delays of up to 5 ms has been shown without interneuron doublets, but with interneuron bursts perhaps playing a similar role[23].

Our model predicts (unlike the models of refs 22 and 24) that pyramidal cells and at least some interneuron spikes should occur with near-zero phase lag[6], and that progressive attenuation of pyramidal cell to interneuron excitation should lead to loss of long-range synchrony before loss of local synchrony (Fig. 3). In the neocortex, large basket cells in layer III have relatively long axons contacting pyramidal cells as well as other large basket cells[25]. Such cells might allow our proposed mechanism to underlie long-range synchrony of '40 Hz' oscillations *in vivo*. □

Methods

Transverse 450-μm-thick hippocampal slices[9,10] were prepared from adult male Sprague-Dawley rats and maintained at 35 °C at the interface between warm, wetted O_2/CO_2 and artificial cerebrospinal fluid containing (in mM): NaCl 135, KCl 4, NaH_2PO_4 1.25, $CaCl_2$ 1.5, $MgCl_2$ 0.8, glucose 10. Stimuli: 50 μs, 6–14 V, were delivered via bipolar silver wire electrodes. Interneurons were impaled at the level of stratum pyramidale with glass microelectrodes containing 2 M potassium methylsulphate, resistance 50–70 MΩ. Neurons had resting membrane potentials between −59 and −68 mV and input resistances of 35–45 MΩ. Presumed interneurons fired narrow (base width 2 ms) action potentials with a rapid, monophasic after hyperpolarization, at high frequencies (>400 Hz), with no accommodation on depolarization.

Received 20 June; accepted 26 August 1996.

1. Gray, C. M., König, P., Engel, A. K. & Singer, W. *Nature* **338,** 334–337 (1989).
2. Engel, A. K., König, P., Kreiter, A. K. & Singer, W. *Science* **252,** 1177–1179 (1991).
3. Gray, C. M. *J. Comput. Neurosci.* **1,** 11–38 (1994).
4. Singer, W. & Gray, C. M. *Annu. Rev. Neurosci.* **18,** 555–586 (1995).
5. Soltesz, I. & Deschênes, M. *J. Neurophysiol.* **70,** 97–116 (1993).
6. Bragin, A., Jandó, G., Nádasdy, Z., Hetke, J., Wise, K. & Buzsáki, G. *J. Neurosci.* **15,** 47–60 (1995).
7. Engel, A. K., Kreiter, A. K., König, P. & Singer, W. *Proc. Natl Acad. Sci. USA* **88,** 6048–6052 (1991).
8. Frien, A., Eckhorn, R., Bauer, R., Woelbern, T. & Kehr, H. *Neuroreport* **5,** 2273–2277 (1994).
9. Whittington, M. A., Traub, R. D. & Jefferys, J. G. R. *Nature* **373,** 612–615 (1995).
10. Traub, R. D., Whittington, M. A., Colling, S. B., Buzsáki, G. & Jefferys, J. G. R. *J. Physiol.* **493,** 471–484 (1996).
11. Innocenti, G. M. *Arch. Ital. Biol.* **118,** 124–188 (1980).
12. Ribary, U. *et al. Proc. Natl Acad. Sci. USA* **88,** 11037–11041 (1991).
13. Andersen, P., Silfvenius, H., Sundberg, S., Sveen, O. & Wigström, H. *Brain Res.* **144,** 11–18 (1978).
14. Murakoshi, T., Guo, J.-Z. & Ichinose, T. *Neurosci. Lett.* **163,** 211–214 (1993).
15. Salin, P. A. & Prince, D. A. *J. Neurophysiol.* **75,** 1589–1600 (1996).
16. Llinás, R. R., Grace, A. A. & Yarom, Y. *Proc. Natl Acad. Sci. USA* **88,** 897–901 (1991).
17. Wilson, M. A. & Bower, J. M. *Neural Comput.* **3,** 498–509 (1991).
18. Traub, R. D. & Miles, R. *J. Comput. Neurosci.* **2,** 291–298 (1995).
19. Sik, A., Penttonen, M., Ylinen, A. & Buzsáki, G. *J. Neurosci.* **15,** 6651–6665 (1995).
20. Buhl, E. H. *et al. J. Neurophysiol.* **71,** 1289–1307 (1994).
21. Bauer, R., Brosch, M. & Eckhorn, R. *Brain Res.* **669,** 291–297 (1995).
22. König, P. & Schillen, T. B. *Neural Comput.* **3,** 155–166 (1991).
23. Bush, P. & Sejnowski, T. *J. Comput. Neurosci.* **3,** 91–110 (1996).
24. Eeckman, F. H. & Freeman, W. J. *Brain Res.* **528,** 238–244 (1990).
25. Kisvárday, Z. F., Beaulieu, C. & Eysel, U. T. *J. Comp. Neurol.* **327,** 398–415 (1993).
26. Traub, R. D., Jefferys, J. G. R., Miles, R., Whittington, M. A. & Tóth, K. *J. Physiol.* **481,** 79–95 (1994).
27. Wong, R. K. S. & Prince, D. A. *J. Neurophysiol.* **45,** 86–97 (1981).

ACKNOWLEDGEMENTS. Supported by IBM, the Wellcome Trust, and the Human Frontier Science Program. We thank H. Monyer, R. K. S. Wong, R. Miles, G. Buzsáki, N. Kopell and R. Linsker for helpful discussion, and R. Walkup and J. Jann for advice with parallel computers.

CORRESPONDENCE and requests for materials should be addressed to R.D.T. (e-mail: traub@watson.ibm.com).

Differentiation of adult hippocampus-derived progenitors into olfactory neurons *in vivo*

Jaana O. Suhonen*, Daniel A. Peterson, Jasodhara Ray & Fred H. Gage

Laboratory of Genetics, The Salk Institute, 10010 North Torrey Pines Rd, La Jolla, California 92037-1099, USA

NEUROGENESIS continues throughout adulthood in discrete regions. Proliferative zones include the subependymal zone[1–4], from where progenitors migrate along the rostral migratory pathway to differentiate into neurons in the olfactory bulb[4], and the hippocampal subgranular zone, where they migrate and differentiate into granule neurons[5–7]. Progenitors isolated from adult subependymal zone exhibit *in vitro* neurogenesis when stimulated with epidermal[8,9] or fibroblast growth factor[10]. Cultured adult rat hippocampal progenitors (AHPs) grafted to adult rat hippocampus show site-specific neuronal differentiation[11]. Here we investigate determinants of multipotentiality in the adult central nervous system, by grafting AHPs into homotypic (hippocampus) or heterotypic (the rostral migratory pathway) neurogenic sites or a heterotypic, non-neurogenic site (the cerebellum). We found that grafts into neurogenic, but not non-neurogenic sites, showed neuronal differentiation. Furthermore, AHPs grafted in the rostral migratory pathway migrated into the olfactory bulb, differentiating into tyrosine-hydroxylase-positive neurons, a non-hippocampus phenotype. These results reveal that AHP populations can respond to persistent neuronal differentiation cues in the adult central nervous system.

AHP cells in culture remain uncommitted, with only a small fraction differentiating into cells with mature neuronal or glial phenotypes[11,12]. To test whether AHPs cultured for over two years differentiate *in vivo* in response to endogenous local cues, cells labelled with 5-bromo-2′-deoxyuridine (BrdU), or an adenoviral vector carrying the *lacZ* gene, were grafted to adult rat hippocampus, cerebellum and rostral migratory pathway (RMP) (Fig. 1*a*). Control experiments, in which BrdU- and adenoviral-labelled cells were sonicated or freeze–thawed before grafting, showed no transfer of markers to endogenous cells[11]. The graft position, distribution of AHPs and their fate were examined at one and eight weeks post-grafting using BrdU- and β-galactosidase immunostaining. Immunostaining revealed that AHPs had survived at all time points in each target zone with no tumour formation (Fig. 1*b–g*). Of 75,000 AHPs grafted per site, 27,136 ± 5,924 (mean ± s.e.m.) were present in the olfactory bulb, 35,863 ± 1,123 in the hippocampus, and 26,584 ± 2,323 in the cerebellum 8 weeks after grafting. There was no significant difference (ANOVA, $\alpha = 0.05$) in AHP survival, indicating that graft site does not influence survival.

Examination of cell distribution at one week revealed the dispersion of AHPs in the hippocampus and cerebellum (Fig. 2*a*). However, AHPs in RMP migrated over 2 mm rostrally along the RMP and subependymal zone (SEZ) (Fig. 2*a*), where most (73%) cells were observed in SEZ, with some (19%) in the olfactory granule cell layer and few (8%) in the glomerular cell layer (Table 1*a*). Eight weeks post-grafting, cerebellar AHP distribution did not differ from that at one week (Fig. 2*b*), suggesting that dispersion rather than specific migration was occurring. In hippocampus, AHPs distributed in the CA1–3 regions and dentate gyrus[11]. In the olfactory bulb, AHPs migrated

* Present address: Dept of Neurology and Restorative Neurology, Tampere University Hospital, PO Box 2000, FIN-33521 Tampere, Finland.